JOURNAL OF GEOPHYSICAL RESEARCH: SPACE PHYSICS, VOL. 118, 3007–3016, doi:10.1002/jgra.50288, 2013

Temporal and spatial dynamics of the regions 1 and 2 Birkeland currents during substorms

L. B. N. Clausen,[1] J. B. H. Baker,[2] J. M. Ruohoniemi,[2] S. E. Milan,[3] J. C. Coxon,[3] S. Wing,[4] S. Ohtani,[4] and B. J. Anderson[4]

Received 24 October 2012; revised 19 March 2013; accepted 17 April 2013; published 7 June 2013.

[1] We use current density data from the Active Magnetosphere and Planetary Electrodynamics Response Experiment (AMPERE) to identify the location of maximum region 1 current at all magnetic local times (MLTs). We term this location the R1 oval. Comparing the R1 oval location with particle precipitation boundaries identified in DMSP data, we find that the R1 oval is located on average within 1° of particle signatures associated with the open/closed field line boundary (OCB) across dayside and nightside MLTs. We hence conclude that the R1 oval can be used as a proxy for the location of the OCB. Studying the amount of magnetic flux enclosed by the R1 oval during the substorm cycle, we find that the R1 oval flux is well organized by it: during the growth phase the R1 oval location moves equatorward as the amount of magnetic flux increases whereas after substorm expansion phase onset significant flux closure occurs as the R1 current location retreats to higher latitudes. For about 15 min after expansion phase onset, the amount of open magnetic flux continues to increase indicating that dayside reconnection dominates over nightside reconnection. In the current density data, we find evidence of the substorm current wedge and also show that the dayside R1 currents are stronger than their nightside counterpart during the substorm growth phase, whereas after expansion phase onset, the nightside R1 currents dominate. Our observations of the current distribution and OCB movement during the substorm cycle are in excellent agreement with the expanding/contracting polar cap paradigm.

Citation: Clausen, L. B. N., J. B. H. Baker, J. M. Ruohoniemi, S. E. Milan, J. C. Coxon, S. Wing, S. Ohtani, and B. J. Anderson (2013), Temporal and spatial dynamics of the regions 1 and 2 Birkeland currents during substorms, *J. Geophys. Res. Space Physics*, *118*, 3007–3016, doi:10.1002/jgra.50288.

1. Introduction

[2] Planetary magnetic field lines can be divided into two categories: those that are closed, i.e., connected to the planet in both hemispheres and those that are open, i.e., connected to the planet on only one end and ultimately to the interplanetary medium on the other. Magnetic reconnection is the agent that transforms magnetic field lines from closed to open and vice versa. At Earth, reconnection occurring on the dayside under the influence of the interplanetary magnetic field (IMF) opens magnetic field lines; they are subsequently swept into the magnetospheric tail by the solar wind. Inside the tail, magnetic reconnection can occur, closing previously open magnetic flux and return flow then transports these closed field lines back to the dayside where they can participate in another cycle of reconnection. This cycle is called the "Dungey cycle" [*Dungey*, 1961] and magnetic reconnection is the essential ingredient. The rates of reconnection on the dayside and nightside are highly variable and generally not balanced, hence measuring the amount of open magnetic flux in the magnetosphere and studying its variation in time allows one to estimate the net reconnection rate and characterize the magnetospheric state.

[3] Measuring the amount of open magnetic flux in the magnetosphere is made possible by global observations of the ionospheric projection of the open/closed field line boundary (OCB). The OCB encloses the area of the ionosphere that is threaded by open magnetic flux, which is called the polar cap; hence, the OCB is sometimes called the polar cap boundary (PCB). Because of its geophysical importance, much effort has gone into identifying the OCB in various data sets. *Mishin* [1990] used an inversion technique of ground-based magnetograms similar to the method

[1]Institute for Geophysics and Extraterrestrial Physics, TU Braunschweig, Braunschweig, Germany.
[2]Bradley Department of Electrical and Computer Engineering, Virginia Tech, Blacksburg, Virginia, USA.
[3]Department of Physics and Astronomy, University of Leicester, Leicester, UK.
[4]The Johns Hopkins University Applied Physics Laboratory, Laurel, Maryland, USA.

Corresponding author: L. B. N. Clausen, Institute for Geophysics and Extraterrestrial Physics, TU Braunschweig, Braunschweig, Germany. (l.clausen@tu-bs.de)

2169-9380/13/10.1002/jgra.50288

of *Kamide et al.* [1981] to calculate field-aligned currents (FACs) on a global scale. Assuming that certain currents flow along the OCB [e.g., *Cowley*, 2000], they argue that they can identify the OCB in their current data. Spatial magnetometer coverage is generally quite good in the northern hemisphere, however, the inversion technique also requires as input the global ionospheric conductivity. Modern conductivity models are still unable to accurately reproduce dynamics especially during geomagnetically active periods; they often fail to represent local enhancements due to particle precipitation, which seriously degrades the prediction of the OCB location using this method.

[4] Global observations of the OCB were previously available through identifying the OCB with the poleward auroral emission boundary derived from satellite-borne global auroral imaging [*Craven and Frank*, 1987; *Frank and Craven*, 1988; *Lassen and Danielsen*, 1989; *Elphinstone et al.*, 1990; *Germany et al.*, 1997; *Brittnacher et al.*, 1999]. These studies have shown that there is substantial movement of the auroral emission boundary throughout the substorm cycle, indicating growth and decay of open magnetic flux.

[5] Based on ideas put forward by *Siscoe and Huang* [1985], *Cowley and Lockwood* [1992] and *Lockwood and Cowley* [1992] proposed the expanding/contracting polar cap (ECPC) paradigm. In this theoretical framework the substorm growth phase is associated with enhanced dayside reconnection and hence the increase of open magnetic flux in the magnetosphere. Dayside reconnection perturbs the magnetospheric equilibrium state and as the magnetosphere tries to recover a new equilibrium, the OCB moves equatorward (the polar cap expands) and ionospheric flows are excited. These flows are in the form of two convection cells centered on the dayside. The ionospheric vortical flows drive FACs called the region 1 currents [*Iijima and Potemra*, 1976], again mainly on the dayside. Open magnetic flux is destroyed by nightside reconnection, which in the ECPC is associated with the substorm expansion and recovery phase. During this phase the OCB moves poleward (the polar cap contracts) and because of the rearrangement of magnetic flux during nightside reconnection, ionospheric flows and associated FACs are driven, now mainly on the nightside. One of the major points of the ECPC paradigm is the realization that ionospheric convection is driven by two separate processes, namely dayside reconnection and nightside reconnection. The rates of both processes can be very different leading to a net increase or decrease of open magnetic flux in the system and hence to expansions and contractions of the polar cap and to OCB motion.

[6] *Milan et al.* [2003] showed that the poleward edge of the auroral oval is colocated with the OCB; using an algorithm to extract the location of this boundary from global auroral images and integrating the magnetic flux over the enclosed area allowed them to estimate the amount of magnetospheric open magnetic flux and study its dynamics through the course of two substorm cycles. They found that the increasing size of the polar cap area was consistent with open flux being created when the IMF was oriented southward. Furthermore, decreases in size corresponded to open flux being closed after substorm onset.

[7] Later studies of longer time series spanning several months of data revealed that the average polar cap size was increased during times of elevated levels of Sym-H [*Milan et al.*, 2008]. This indicates that the magnetotail is more stable and can accumulate more open magnetic flux during intervals of enhanced ring current strength. Separating about 2000 substorms into groups depending on the onset latitude, i.e., according to the amount of open flux inside the magnetosphere, *Milan et al.* [2009] found that those at lower latitudes were more intense in terms of auroral brightness, and their magnetic flux closure was more significant. *Grocott et al.* [2009] conducted a superposed epoch analysis of ionospheric convection during 1979 substorms and found that low latitude onsets are associated with stronger convection flows and also suffer from a localized flow reduction at the location of auroral onset. They attribute the reduction in flow speed to a localized increase in ionospheric conductivity due to particle precipitation.

[8] Also, using global auroral imaging data to compare the amount of open flux during substorms with those during steady magnetospheric convection events (SMCs), *Dejong et al.* [2007] showed that during substorms the amount of open flux changed whereas SMCs are characterized by a stable flux amount and hence appear to have balanced dayside and nightside reconnection rates.

[9] In this paper we investigate the dynamics of both the amount of open magnetic flux by proxy of the region 1 current location and the polar field-aligned current distribution during the substorm cycle. We will show that our observations are in excellent agreement with predictions made by the ECPC paradigm.

1.1. The AMPERE Data Set

[10] The Iridium® constellation consists of 66+ commercial satellites in 780 km polar circular orbits distributed over six orbital planes to provide global satellite telephone and data service. Each satellite carries an engineering magnetometer as part of its attitude system, and *Anderson et al.* [2000] showed that combining 2 h of magnetic field perturbation data from all satellites allows one to estimate the global distribution of radial current densities [see also *Anderson et al.*, 2002]. In the polar regions, i.e., at magnetic latitudes >60°, these radial currents correspond to the Birkeland currents or field-aligned currents (FACs) commonly associated with the region 1 (R1) and region 2 (R2) current system [*Iijima and Potemra*, 1978; *Cowley*, 2000]. Prior to January 2010, the engineering magnetometer data was telemetered to the ground with coarse time resolution (200 s per sample) such that the data had to be accumulated over long periods of time, about 2 h, to acquire a composite sample of the magnetic signatures in the polar regions. This limitation has been resolved under the Active Magnetosphere and Planetary Electrodynamics Response Experiment (AMPERE). AMPERE is a facility funded by the National Science Foundation that increased the time resolution of the magnetic perturbation data provided by the Iridium® satellites by a factor of 10 to 20 s/sample during normal mode and by a factor of 100 in high-rate sampling when the resolution is increased to 2 s/sample. This allows the global radial current density to be estimated every 2 min, although the true update rate is 10 min commensurate with the intersatellite time spacing in each orbit plane. The data used here was provided with a longitudinal resolution of 1 h magnetic local time (MLT), i.e., the resolution is double that provided

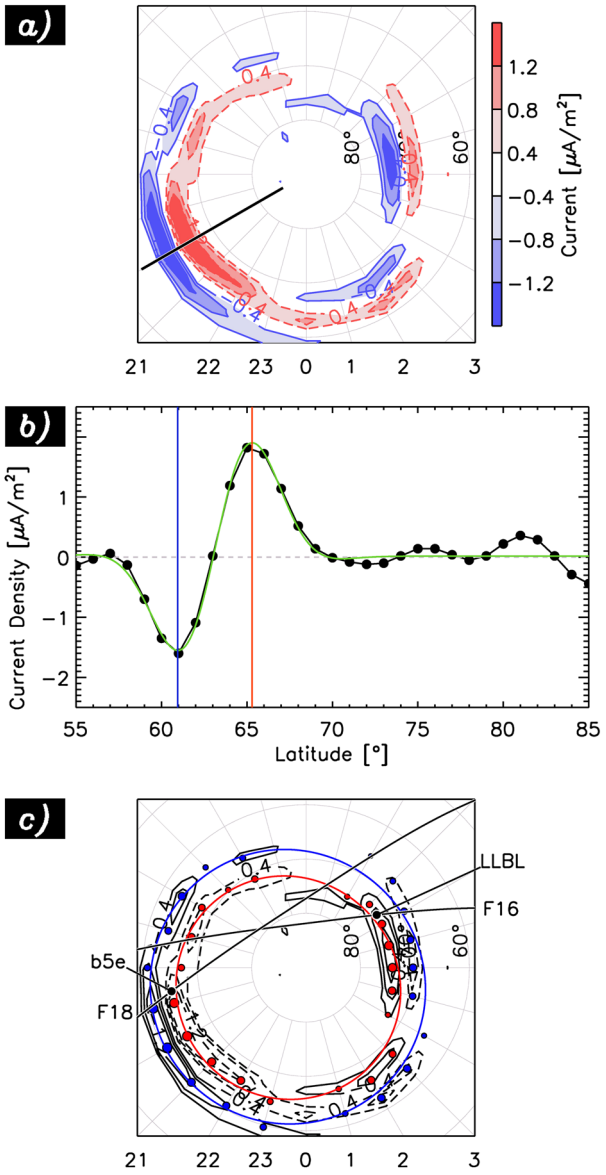

Figure 1. (a) The AMPERE current densities from 01 March 2011, 1230 UT, over the northern hemisphere in magnetic latitude/magnetic local time (MLT) coordinates. The sun is located to the top of the figure. Currents into and out of the ionosphere are colored blue and red, respectively. (b) The measured current densities are shown as black dots, the fit to identify the location of the maximum (red line) and minimum (blue line) current is shown in green. (c) The result of the second fit, the R1/R2 oval is colored red/blue, respectively. Two concurrent DMSP passes are shown as black lines and the location of the b5e and LLBL boundary are marked as black dots. See text for further details.

by the orbit plane spacing of the spacecraft. The sampling rate limits the latitudinal resolution and in normal mode the AMPERE data are spaced by 1° in magnetic latitude. The fitted data used in this study are publicly available from the project Web site at http://ampere.jhuapl.edu.

2. The R1 Oval and the OCB

[11] In a study of AMPERE current density distributions during two individual events, the R1/R2 oval was defined by *Clausen et al.* [2012] as the location of the maximum R1/R2 current above the polar ionosphere. We use the algorithm described in *Clausen et al.* [2012] to extract the R1/R2 oval from the AMPERE vertical current data. Briefly, the algorithm first locates the maximum R1/R2 current in 24 latitudinal current profiles at each MLT, and then the 24 MLT/latitude positions of the maximum current are fitted by a circle to give an estimate of the maximum R1/R2 current location at all magnetic local times. This process is illustrated in Figure 1. Figure 1a shows a map of the vertical currents measured by AMPERE over the northern hemisphere on 01 March 2011, 1230 UT; currents into and out of the ionosphere are colored blue and red, respectively. We also show as a black line the location of the latitudinal current profile shown in Figure 1b. By fitting an appropriate function to this current profile—in Figure 1b, the measured currents are shown as black dots, the fitted function is shown as a green line—the maximum and minimum current, highlighted by vertical red and blue lines, are located. According to the MLT of the current profile, the maximum/minimum current is identified as the R1/R2 current on the dusk side ($12 \leq \mathrm{MLT} < 24$) and as the R2/R1 current on the dawn side ($00 \leq \mathrm{MLT} < 12$). If the fit returns an R1 current location that is equatorward of the R2 current, that fit is rejected. If more than five current profiles were fit successfully, these R1 and R2 MLT/latitude pairs are fitted individually by a circle to yield the location of the two current ovals. The R2 and R1 ovals are shown in Figure 1c in blue and red, respectively. The black contours in Figure 1c again show the vertical current distribution measured by AMPERE.

[12] *Clausen et al.* [2012] showed qualitatively that the size of the R1 oval undergoes expansions and contractions in sync with the substorm cycle: prior to substorm onset, the R1 oval size increased, indicating that the R1 current was pushed to lower latitudes as dayside reconnection added magnetic flux to the polar cap. After substorm onset, as nightside reconnection caused a decrease of open magnetic flux in the magnetosphere, the R1 oval shrank, i.e., the R1 current receded poleward. As the OCB is expected to behave in the same fashion, i.e., move equatorward during expansion phase and poleward during the recovery phase, it is reasonable to assume that the R1 oval location is somehow related to the location of the OCB. One method of localizing the OCB locally is by automatically identifying certain characteristics of precipitating particles in energy spectra measured along the sun-synchronous orbits of the DMSP satellites. The automatic identification of the OCB in DMSP particle data on the nightside is quite straightforward. It is usually believed to align with the b5i and b5e boundaries [*Newell et al.*, 1996]. These boundaries are identified by looking for sharp spatial drop-offs in the electron energy spectra (b5e) and ion energy spectra (b5i), and they mark the poleward edge of the main auroral oval. Hence, on the nightside, we are going to compare the R1 oval location to the location of the b5e and b5i boundaries [*Ohtani et al.*, 2010].

[13] Particle spectra on the dayside provide information about the origin of precipitating particles, however, whether the origin is located on open or closed field lines is

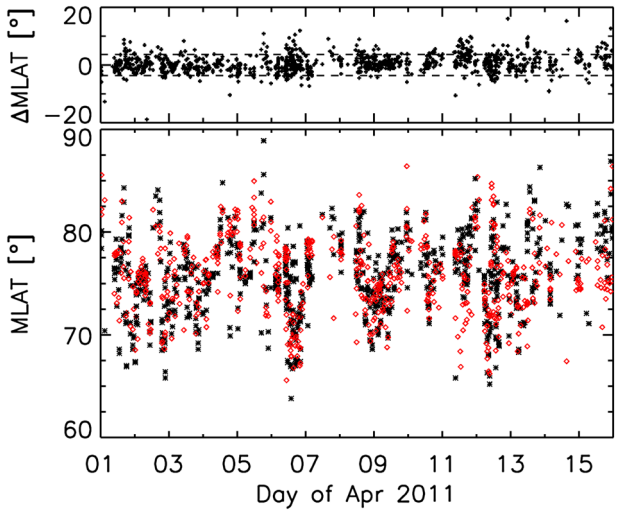

Figure 2. (bottom) Fifteen days of R1 oval locations (red diamonds) and DMSP boundaries (black crosses) between 01 April and 15 April, 2010, both on the dayside and nightside. (top) The latitudinal difference for each boundary pair. Horizontal dashed lines are drawn at the rms error of the latitude differences.

sometimes unclear. Here we chose to compare the R1 oval location to the locations of three regions, which are generally considered to locate closely to the dayside OCB: the mantle, the cusp, and the low-latitude boundary layer (LLBL). The localization of each due to the characteristics of the precipitating particles is based on the analysis by *Wing et al.* [2010]. The mantle and the cusp have been associated with open magnetic field lines, whereas the LLBL is sometimes on open and sometimes on closed magnetic field lines [*Wing et al.*, 1996, 2001, 2005].

[14] For each successful determination of the R1 oval from AMPERE data between 01 January 2010 and 31 August 2011, we search a list of all identified boundaries in DMSP particle spectra to find those DMSP boundaries which were identified within ±4 min of the R1 oval determination. If more than one DMSP boundary was found within this time span, we choose the one that is closest in time. The R1 oval latitude at the MLT closest to the DMSP orbital path is then saved together with the DMSP boundary latitude and other information, e.g., the type of the DMSP boundary. In Figure 1c, we show the pass of two DMSP satellites (F16 and F18) across the northern hemisphere as black lines. We also mark the location of the b5e boundary identified on the nightside by F18 and the location of the LLBL on the dayside as identified by F16. This example shows the excellent agreement on this occasion between the R1 oval location and the DMSP boundaries both on the dayside and the nightside.

[15] This method of comparing boundaries from AMPERE and DMSP yields a list of locations, pairing an R1 oval location with the position of a DMSP boundary. In Figure 2 bottom, we show the magnetic latitudes of these pairs, the R1 oval location is shown as a red diamond, the DMSP boundary is shown as a black cross. In Figure 2, we show all boundary pairs found between 01 April and 15 April, 2010, both on the dayside and nightside. Other periods show the same general characteristics as shown in Figure 2; we chose this period because it contains a rather large amount of data due to larger geomagnetic activity and hence stronger R1 currents. This positively influences the R1 oval determination scheme. In Figure 2top, we plot the latitudinal difference of each boundary pair; horizontal dashed lines are drawn at the rms error of the latitude differences which for this period was about 3°. Figure 2 shows that the latitudinal offset between DMSP boundary and R1 oval location is generally below 3°; large variations in the boundary locations are observed during this period, however, the latitudinal offset between the boundaries is rather constant.

[16] We now extend the boundary comparison analysis to the entire AMPERE data set between 01 January 2010 and 31 August 2011. On the dayside, we find 14,948 contemporaneous boundary/oval determinations, on the nightside, we find 15,801 and for each we calculate the latitudinal offset between the DMSP boundary and the R1 oval. A positive/negative offset indicates that the DMSP boundary is located poleward/equatorward of the R1 oval, respectively. We then calculate the lower quartile, median, and upper quartile of the latitudinal offsets in 1 h MLT bins for each of the two boundaries on the nightside and the three boundaries on the dayside. The results are shown in Figure 3. The offsets on the nightside are shown in Figure 3top, Figure 3bottom shows the offsets for the dayside boundaries. Different colors denote different boundaries, and the numbers underneath the data points give the number of boundary pairs in each MLT bin.

[17] Figure 3top shows that on the nightside, the b5i/e boundaries tend to locate about 1° poleward of the R1 oval, and the median as well as the spread of the offsets is quite constant over all MLTs. The ion and electron boundary tend to colocate. On the dayside (see Figure 3bottom), we find that the location of mantle precipitation tends to lie 3–4° poleward of the R1 oval, with quite large spread of the data values. The LLBL is seen to almost colocate with the R1

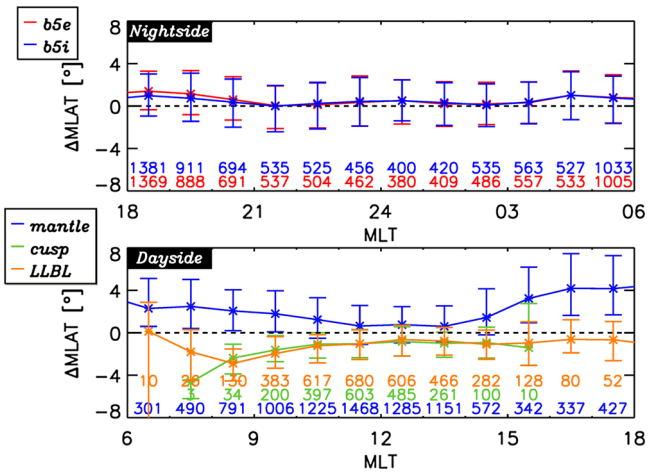

Figure 3. The figure shows the upper quartile, median, and lower quartile of the latitudinal offsets between the R1 oval and the DMSP boundaries, on the (top) nightside and on the (bottom) dayside. The number of boundary comparisons of which the median and quartiles were determined for each MLT bin is given underneath the data points in the same color as the DMSP boundary.

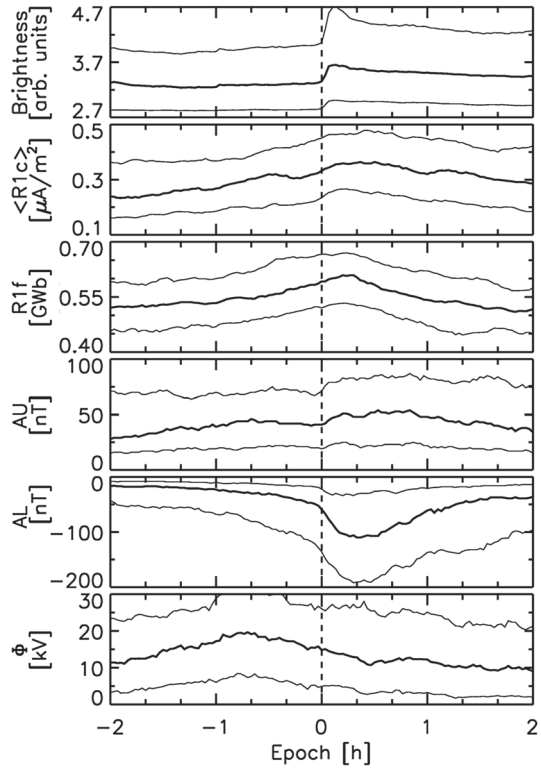

Figure 4. Superposed epoch analysis of magnetospheric and solar wind parameters, keyed on the substorm expansion phase onset time T_0 identified from all-sky imager data for 772 substorms identified between January and April 2010. From top to bottom we show the integrated auroral brightness, the current density averaged over the northern R1 oval, the magnetic flux enclosed by the R1 oval in the northern hemisphere, the AU and AL auroral indices, and the dayside reconnection potential.

oval to within 1°, with an exception between seven and eight MLT; this exception, however, could be due to poor statistics. The LLBL tends to lie equatorward of the R1 oval. At those MLTs where the location of the cusp precipitation is available, it is seen to colocate both with the LLBL and the R1 oval, to within about 1° when good statistics are available.

[18] We have shown that the R1 oval is closely coincident to proxies for the OCB determined from DMSP observations, it is hence quite reasonable to use the amount of magnetic flux enclosed by the R1 oval R1f as a proxy for the amount of open magnetic flux in the magnetospheric system. We calculate the amount of open magnetic flux R1f by integrating the vertical component of the International Geomagnetic Reference Field (IGRF) over the area enclosed by the R1 oval.

3. Substorm Observations

[19] Having established that statistically the R1 oval is related to the OCB, we can now investigate the dynamics of the open magnetic flux during the substorm cycle by studying the motion of the R1 oval. To achieve this, we perform a superposed epoch analysis of relevant parameters keyed on substorm expansion onset time T_0. A list of expansion phase onsets between January 2010 and April 2010 identified in all-sky imagers located across the northern US and Canada is available on the Web site of the THEMIS mission. This list contains 829 onsets, and for 772 of those events, we are able to determine the R1 oval using the technique described above. Sometimes the same onset is observed by multiple imagers. Figure 4 shows the result of our superposed epoch analysis for the 772 substorm onsets. The thick lines give the medians of the distributions, the thin lines give the upper and lower quartiles. From top to bottom we show the integrated brightness in the all-sky imager data, the median R1 current along the northern R1 oval, the magnetic flux inside the northern R1 oval, the AU and AL auroral indices, and finally the geoeffective electric potential. $\langle \mathrm{R1c} \rangle$ is calculated as the R1 current located on the R1 oval averaged over all MLTs; because of the different polarity of the R1 currents on the dusk and dawn side, we take the average of the absolute current density along the R1 oval. We calculate the last parameter Φ, also known as the rate of dayside reconnection, following *Milan et al.* [2012] as

$$\Phi = \Lambda\, v_X^{4/3} \sqrt{B_Y^2 + B_Z^2}\, \sin^{9/2}\left(\frac{\theta}{2}\right) \tag{1}$$

where v_X is the solar wind speed in the GSM X direction, B_Y/B_Z are the IMF components in the GSM Y/Z direction, and θ is the IMF clock angle, i.e., the angle between the IMF direction and the GSM Z direction. If B_Z is positive, we set Φ equal to zero. For the characteristic scale length Λ we use $3.8R_e/(4 \times 10^5 ms^{-1})^{1/3}$ [*Milan et al.*, 2012]. As input for Φ we use the OMNI solar wind data which is time shifted to the subsolar bow shock.

[20] In Figure 4, we only show the average R1 current and enclosed magnetic flux for the northern hemisphere measurement, and in the following, we will only discuss these values for the northern hemisphere. Figure 4 shows that following expansion phase onset, which is marked as a vertical dashed line, the auroral brightness measured by the all-sky imagers abruptly increases. Prior to onset, both the R1 current average over the R1 oval location $\langle \mathrm{R1c} \rangle$ and the magnetic flux enclosed by the R1 oval R1f had increased over a period of about 1 h. This behavior is expected of the substorm growth phase, which is accompanied by an increase in Φ, indicating a higher dayside reconnection rate prior to T_0. A slight increase in AU and a slight decrease in AL are also observed during the 2 h leading to substorm onset.

[21] Following the auroral brightening, the average R1 current further increases before reaching its maximum about 20 min after expansion phase onset and then it decreases to about its pre-onset value. The amount of open magnetic flux also continues to increase after expansion phase onset, peaking around 15 min after T_0 and about 5 min after the time of maximum auroral brightness. The growth of the magnetic flux inside the R1 oval is followed by a decrease of the amount of open magnetic flux in the magnetosphere by about 0.1 GWb (in the northern hemisphere) during the substorm expansion and recovery phase. After T_0 the AU index slightly decreases again whereas the AL index shows a distinct negative bay, as expected for substorm onset. About 20 min after T_0, the dayside reconnection voltage has recovered to its pre-onset value and stays on that value throughout the rest of the substorm cycle.

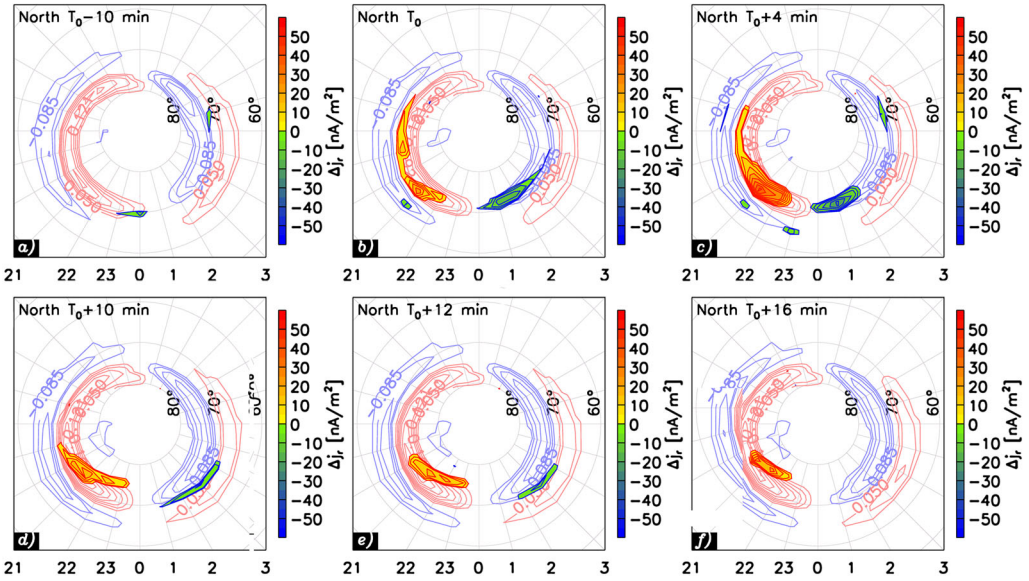

Figure 5. Superposed epoch analysis of the AMPERE vertical current densities at selected times relative to substorm expansion phase onset T_0 for 772 substorm expansion phase onsets between January 2010 and April 2010. The non-filled contours give the average vertical current densities. Downward currents are colored blue, upward currents are colored red. As filled contours, we show the magnitude of the current change with respect to the distribution 6 min earlier. Although the large-scale currents do not change significantly, it can be seen that after substorm onset the R1 currents become more downward in the post-midnight sector and more upward in the pre-midnight sector, consistent with the sense of the substorm current wedge.

[22] So far, we have established that statistically the R1 oval location is related to the position of the OCB and that the R1 oval movement mirrors that expected of the OCB during the different phases of the substorm cycle. We will now turn to the R1 and R2 currents and their behavior during the different phases of the substorm. First, we use the global vertical current density distributions provided by AMPERE to calculate superposed epoch current maps. Centered around expansion phase onset T_0, we average the current densities at each point of the AMPERE grid for the time between $T_0 - 2$ h and $T_0 + 2$ h. Resulting current maps in the northern hemisphere in a magnetic latitude/MLT coordinate system are shown in Figure 5 for selected times around onset.

[23] In Figure 5 we show the average current density in a magnetic latitude/MLT grid in the northern hemisphere. The time of the map relative to T_0 is given in the top left corner of each panel. Note that we have not rotated or scaled the original current density maps to achieve a single substorm onset location prior to averaging. The current densities are shown as non-filled colored contours, upward currents in red and downward currents in blue. The average current strength is weak, only about 0.2 $\mu A/m^2$, but a clear signature of the R1/R2 current distribution is observed throughout the 30 min interval shown. Although the current distribution is somewhat variable during the period shown here, the overall shape of the two concentric rings of current is maintained across the expansion phase onset. In particular, in the average currents there is no obvious signature of the substorm current wedge (SCW).

[24] However, we also calculate the magnitude of the change in current density at each point on the grid between current maps 6 min apart. This current density difference we show as filled contours, the colors varying according to the color bar on the right of each panel in Figure 5. Using this technique, we clearly see a change in the nightside R1 currents on this time scale, starting at onset and disappearing about 20–30 min later. We see that on average, the R1 current in the pre-midnight sector becomes more positive, i.e., more upward (yellow-red), whereas in the post-midnight sector the R1 current density decreases, i.e., becomes more downward (green-blue). This is indeed consistent with the expected sense of the SCW [*McPherron et al.*, 1973].

[25] To investigate whether and when currents on the dayside or currents on the nightside dominate, we first apply the fitting technique described in *Clausen et al.* [2012] to the averaged current density maps, some of which are shown in Figure 5. With this technique we can extract the average—in a superposed epoch sense—location and strength of the R1/R2 current system. Using these averaged fitted current densities, we calculate the average dayside current $\langle j_{rD} \rangle$ as the median of the currents on the R1/R2 oval between 07 and 17 MLT, taking into account the different polarities of the currents on the dawn and dusk flanks. Similarly, we determine the average nightside current $\langle f_{rN} \rangle$ as the average of the R1/R2 oval currents between 19 and 05 MLT. To investigate whether the dayside or the nightside current dominates, we then calculate the ratio between the dayside current $\langle j_{rD} \rangle$ and the nightside current $\langle f_{rN} \rangle$. A ratio of 1 indicates equal amounts of dayside and nightside current, a ratio smaller/greater than 1 is showing greater nightside/dayside currents. We perform this analysis at each time step of our superposed epoch analysis to yield a time series of the dayside to night current ratio. In the top two panels of Figure 6, we show $\langle j_{rD} \rangle / \langle j_{rN} \rangle$ for the R1 currents on the left and for the R2 currents on the right side.

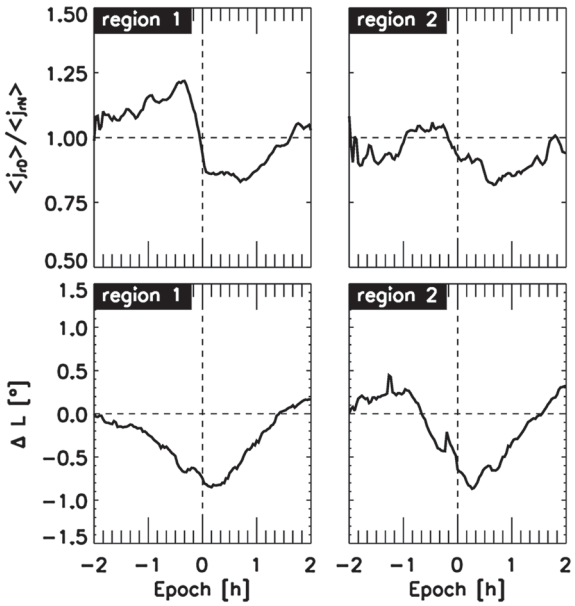

Figure 6. (top) The ratio between the average dayside and nightside currents for the R1 (left) and R2 (right) current system. (bottom) The location of the current, again for the R1 current system on the left and the R2 current system on the right.

[26] Figure 6 shows that during the substorm growth phase, the dayside currents are stronger. At their maximum between 60 and 30 min prior to onset, the dayside currents are about 25% stronger than the nightside currents. During the expansion phase, the nightside currents dominate, being about 20%–25% larger. The ratio of the R2 currents also shows some interesting dynamics, however, we observe no apparent pattern. The dayside current density is smaller during the substorm growth phase than during the expansion and recovery phase. This might be a seasonal effect, considering that the substorms studied here occurred exclusively in southern hemisphere summer.

[27] In the bottom row of Figure 6, we show the latitudinal movement of the fitted R1 and R2 oval, average over all MLTs. At each time t, the change in latitude ΔL is calculated as the current latitude at time t minus the current latitude at time $T_0 - 2$ h. We observe that both the R1 and R2 currents move to lower latitudes before the expansion phase onset, indicated by negative ΔL. Note that the movement of the currents starts about 20–30 min after the increase in current density. Shortly after T_0 both the R1 and R2 ovals contract, as indicated by a decreasing ΔL.

4. Discussion

[28] The method described in *Clausen et al.* [2012] allows one to extract the location of the maximum R1 current from AMPERE current density data. *Clausen et al.* [2012] show that, if the R1/2 current system is reasonably strong, i.e., if the average peak current density in the R1/2 system exceeds $0.2\mu A/m^2$, the location of the maximum R1 current can be determined to within 1° accuracy. Previous studies by *Wing et al.* [2010] and *Ohtani et al.* [2010] have shown that the location of the R1 currents are usually closely related to the location of the OCB. Both studies use magnetic field perturbation data measured onboard the DMSP satellites to identify FACs and hence the R1/R2 currents and they relate their location with concurrent particle precipitation measurements. In this study, we essentially do the same, however, instead of using FAC data measured along a DMSP orbit, we compare the precipitation boundaries to locations of the R1 currents automatically extracted from the global AMPERE data set. We find that, statistically, the R1 currents are located about 1° equatorward of the OCB on the nightside, and within 1° on the dayside, which is in good agreement with the results obtained by *Wing et al.* [2010] and *Ohtani et al.* [2010]. Our results suggest that the R1 oval location can be used as a proxy for the OCB in a statistical sense, however, during individual events the latitudinal difference between the R1 current location and the DMSP particle precipitation boundaries can become rather large, in some cases exceeding 5°; the comparison between DMSP boundaries and AMPERE current locations shown in Figure 2 illustrates this. When taking into account every boundary comparison in our data set, regardless of dayside or nightside and regardless of particle boundary type, we find, in agreement with Figure 3, that the median latitudinal offset between the DMSP boundary and the R1 oval is 0.73°, i.e., the R1 oval is located about 1° equatorward of the DMSP boundary. We also find that the upper and lower quartile of all latitude offsets is –1.18° and 2.90°, respectively. These numbers show that in 50% of all boundary comparisons, the difference is below ±2°. Suppose the location of the OCB is misjudged by 2° in magnetic latitude at all MLTs, such that the OCB is located at 75° MLAT whereas the AMPERE data suggests it is located at 73° MLAT, the difference in the estimate of the amount of open magnetic flux is about 30%. While DMSP measurements might be preferred to accurately find the location of the OCB, they can only do so at one particular MLT; AMPERE has, in stark contrast to DMSP magnetometer and particle data, the benefit that it provides global estimates of the FAC distribution and hence the OCB, simultaneous in both hemispheres.

[29] The good spatial correlation between the R1 oval and OCB then allows us to integrate the magnetic flux inside the R1 oval and claim reasonable agreement, at least statistically, of that value with the instantaneous amount of open magnetic flux in the magnetosphere. *Milan et al.* [2007] demonstrated that typical substorms close about 0.3 GWb of magnetic flux. The average change in open magnetic flux that we infer is about 0.1 GWb in the northern hemisphere, using the technique described above during 772 substorms occurring between January 2010 and April 2010. We are also able to show that the current densities of the R1 oval tend to increase during the substorm growth phase and peak about 10 min after substorm onset. In our analysis, the IMF B_Z component is most negative during the substorm growth phase such that the increase in current density during this period also agrees with the statistical results of the R1/R2 current strength presented by *Anderson et al.* [2008].

[30] For about 15 min after expansion phase onset, the amount of open magnetic flux continues to increase indicating that dayside reconnection continues to dominate over nightside reconnection. During this period when the open magnetic flux continues to increase, we find signatures of the substorm current wedge in the superposed epoch averaged

AMPERE data. However, it is a rather weak feature in the original data; it only clearly shows up in maps of the current density change until about 20 min after onset. The fact that a SCW signature is observed in our analysis shows that, in a statistical sense, the SCW location is quite stable. This is consistent with observations by *Frey et al.* [2004] which show that the MLT distribution of auroral breakups is wide, but their occurrence is not random in MLT; instead, they do have a preferred MLT sector and are centered around 23 MLT. Note that the current data was not rotated or scaled to superpose all substorm onset locations such that spatial averaging might produce an underestimate of the actual current. Integrated over the area in which the SCW is observed, the average total current carried by the SCW is estimated to lie around 0.1 MA. Our estimate is substantially lower than early values inferred using ground based magnetometer signatures [*Clauer and McPherron*, 1974]. However, modeling suggests that induced ionospheric currents amplify the ground signature of the SCW and that the actual current carried by the SCW is about a factor of 10 smaller than the early estimates of 2 MA [McPherron, private communication].

[31] Our analysis shows that the SCW, especially the pre-midnight upward current, at substorm expansion phase onset (T_0, see Figure 5b) is located just equatorward of the strongest R1 current. This is consistent with previous studies that show that the auroral breakup, i.e., the initial auroral brightening at substorm expansion phase onset, takes place at the equatorward most arc [*Akasofu*, 1964]. It is furthermore consistent with observations by *Ohtani et al.* [2010], which show that b3a, i.e., the location of the most equatorward electron acceleration, occurs in the vicinity of the R1/R2 demarcation in the dusk-to-midnight sector. Following substorm expansion phase onset, the auroral bulge develops and proceeds poleward [e.g., *Fujii et al.*, 1994]. The poleward retreat of the upward part of the SCW located in the pre-midnight sector, associated with downgoing electrons and hence auroral activity, is also observed in our superposed epoch analysis shown in Figure 5. It should be noted that we find no evidence of a secondary wedge at latitudes below the SCW with opposite polarity [*Birn et al.*, 1999].

[32] The last part of our analysis looks into the ratio between dayside and nightside currents during the substorm cycle. During the substorm growth phase, dayside currents are about 25% stronger than nightside currents. At the same time, as the dayside currents dominate the overall R1 and R2 current, oval moves to lower latitudes. After substorm expansion phase onset, the dominance shifts toward the nightside currents and the R1 and R2 current ovals recede poleward. All of these observations are consistent with the expanding/contracting polar cap (ECPC) paradigm put forward by *Cowley and Lockwood* [1992] and *Lockwood and Cowley* [1992] and also confirmed by modeling [S. E. Milan, Modelling Birkeland currents in the expanding/contracting polar cap paradigm, submitted to *Journal of Geophysical Research Space Physics*, 2013]. In this paradigm, dayside reconnection adds open magnetic flux to the polar cap. The addition of new open magnetic flux disturbs the magnetospheric equilibrium state and in its effort to attain a new equilibrium vortical ionospheric flows, predominantly on the dayside, are excited. These vortical flows in turn drive the FACs that are the R1 currents, again, mainly on the dayside. Furthermore, the addition of new open flux to the essentially incompressible ionosphere pushes the boundary between open and closed magnetic flux—close to which the R1 current system is located—equatorward. We observed both the dayside dominance of the R1 currents and the equatorward expansion of the OCB. Substorm expansion phase onset is caused by a sudden increase in nightside reconnection. In the ECPC paradigm, again, the magnetospheric equilibrium state is perturbed and consequently ionospheric convection is driven, now predominantly on the nightside, leading to stronger R1 currents on the nightside. As open magnetic flux is destroyed in this process, the OCB and the R1 currents flowing along it move poleward. Again, this is confirmed by our observations. We should also note that our observations show that the R2 current strength is, as predicted by the ECPC, not affected by the rates of reconnection either on the dayside or the nightside. Its location, however, shifts through the substorm cycle in order to accommodate the motion of the OCB and hence the R1 current system. This imbalance of R1 current is one of the central predictions of the ECPC paradigm, which has not been addressed in the literature before, simply because direct measurements of the global FAC system were not available prior to AMPERE.

[33] Due to its dependence on auroral imaging in the northern hemisphere, in this study, we use AMPERE data from January to April. During this time the conductance is higher in the sunlit summer, the southern hemisphere. *Ohtani et al.* [2005] have shown that the dayside R1 currents into the summer hemisphere are significantly higher than into the winter hemisphere, and indeed, we see this in our study. However, the dayside/nightside asymmetry shown in Figure 6 is not due to this semiannual variation, as the different timescales clearly indicate.

5. Summary

[34] By comparing with precipitation boundaries observed by DMSP satellites, we have shown that the positions of the R1 current automatically extracted from AMPERE data can be used, statistically, as a proxy for the OCB. With this knowledge, we can integrate the magnetic flux inside the oval enclosed by the R1 currents and relate that quantity to the open magnetic flux in the magnetosphere. Indeed, when studying dynamics of the magnetic flux inside the R1 oval, R1f, during the substorm cycle, we find that it increases during the substorm growth phase indicating that open magnetic flux is created by dayside reconnection. This interpretation is confirmed by the observation of higher dayside reconnection potentials prior to onset. After the substorm expansion phase onset, R1f decreases, as would be expected when nightside reconnection converts open magnetic flux previously stored in the magnetotail to closed magnetic flux. Interestingly, R1f continues to increase for several minutes after onset before it begins to decrease, indicating that it takes some time for nightside reconnection to overtake the dayside reconnection in converting magnetic flux.

[35] Having established that the substorms studied here indeed open and close magnetic flux, we turn to investigate the regional and large-scale current systems associated with the substorm phases in a superposed epoch sense. We find

signatures of the SCW which appears at substorm expansion phase onset on top of the R1 current location that lasts about 20 min. We estimate the total current carried by the SCW to about 0.1 MA. Our analysis also shows that prior to substorm onset, as open magnetic flux is added to the polar cap and the OCB moves equatorward, R1 currents are stronger on the dayside. After substorm expansion phase onset, the nightside part of the R1 current system dominates, and the OCB retreats poleward. The large-scale coverage provided by AMPERE for the first time offers the opportunity to show by direct observation the movement of the regions 1/2 current system associated with the substorm phases and the 2D spatial extent of the SCW. Our findings suggest that the ECPC paradigm indeed provides the framework with which to describe the dynamics of R1/R2 currents and ionospheric convection during the substorm cycle.

[36] **Acknowledgments.** The authors would like to thank the THEMIS all-sky imager team for providing a list of substorm expansion phase onsets on their mission Web site at ftp://justice.ssl.berkeley.edu/events. L.B.N.C. acknowledges funding from the National Science Foundation under grant ATM-0924919 and from the Deutsches Zentrum fuer Luft- und Raumfahrt under grants 50OC1102 and 50OC1001. S.E.M. was supported by the Science and Technology Facilities Council (STFC), UK, grant ST/H002480/1. J.C.C. was supported by an STFC studentship. The authors from Virginia Tech thank the National Science Foundation for support under grant AGS-0946900.

[37] Robert Lysak thanks Martin Connors and another reviewer for their assistance in evaluating this paper.

References

Akasofu, S.-I. (1964), The development of the auroral substorm, *Planet. Space Sci.*, *12*, 273–282, doi:10.1016/0032-0633(64)90151-5.

Anderson, B. J., K. Takahashi, and B. A. Toth (2000), Sensing global Birkeland currents with Iridium® engineering magnetometer data, *Geophys. Res. Lett.*, *27*, 4045–4048, doi:10.1029/2000GL000094.

Anderson, B. J., K. Takahashi, T. Kamei, C. L. Waters, and B. A. Toth (2002), Birkeland current system key parameters derived from Iridium® observations: Method and initial validation results, *J. Geophys. Res.*, *107*(A6), 1079, doi:10.1029/2001JA000080.

Anderson, B. J., H. Korth, C. L. Waters, D. L. Green, and P. Stauning (2008), Statistical Birkeland current distributions from magnetic field observations by the Iridium® constellation, *Ann. Geophys.*, *26*, 671–687, doi:10.5194/angeo-26-671-2008.

Birn, J., M. Hesse, G. Haerendel, W. Baumjohann, and K. Shiokawa (1999), Flow braking and the substorm current wedge, *J. Geophys. Res.*, *104*, 19,895–19,904, doi:10.1029/1999JA900173.

Brittnacher, M., M. Fillingim, G. Parks, G. Germany, and J. Spann (1999), Polar cap area and boundary motion during substorms, *J. Geophys. Res.*, *104*, 12,251–12,262, doi:10.1029/1998JA900097.

Clauer, C. R., and R. L. McPherron (1974), Mapping the local time-universal time development of magnetospheric substorms using mid-latitude magnetic observations, *J. Geophys. Res.*, *79*(19), 2811–2820, doi:10.1029/JA079i019p02811.

Clausen, L. B. N., J. B. H. Baker, J. M. Ruohoniemi, S. E. Milan, and B. J. Anderson (2012), Dynamics of the region 1 Birkeland current oval derived from the Active Magnetosphere and Planetary Electrodynamics Response Experiment (AMPERE), *J. Geophys. Res.*, *117*, A06233, doi:10.1029/2012JA017666.

Cowley, S. W. H. (2000), *Magnetosphere-ionosphere interactions: A tutorial review*, 91–106, Magnetospheric Current Systems.

Cowley, S. W. H., and M. Lockwood (1992), Excitation and decay of solar wind-driven flows in the magnetosphere-ionosphere system, *Ann. Geophys.*, *10*, 103–115.

Craven, J. D., and L. A. Frank (1987), Latitudinal motions of the aurora during substorms, *J. Geophys. Res.*, *92*, 4565–4573, doi:10.1029/JA092iA05p04565.

Dejong, A. D., X. Cai, R. C. Clauer, and J. F. Spann (2007), Aurora and open magnetic flux during isolated substorms, sawteeth, and SMC events, *Ann. Geophys.*, *25*, 1865–1876, doi:10.5194/angeo-25-1865-2007.

Dungey, J. W. (1961), Interplanetary magnetic field and the auroral zones, *Phys. Rev. Lett.*, *6*, 47–48.

Elphinstone, R. D., K. Jankowska, J. S. Murphree, and L. L. Cogger (1990), The configuration of the auroral distribution for interplanetary magnetic field Bz northward. I - IMF Bx and By dependencies as observed by the Viking satellite, *J. Geophys. Res.*, *95*, 5791–5804, doi:10.1029/JA095iA05p05791.

Frank, L. A., and J. D. Craven (1988), Imaging results from Dynamics Explorer 1, *Rev. Geophys.*, *26*, 249–283, doi:10.1029/RG026i002p00249.

Frey, H. U., S. B. Mende, V. Angelopoulos, and E. F. Donovan (2004), Substorm onset observations by IMAGE-FUV, *J. Geophys. Res.*, *109*, A10304, doi:10.1029/2004JA010607.

Fujii, R., R. A. Hoffman, P. C. Anderson, J. D. Craven, M. Sugiura, L. A. Frank, and N. C. Maynard (1994), Electrodynamic parameters in the nighttime sector during auroral substorms, *J. Geophys. Res.*, *99*, 6093–6112, doi:10.1029/93JA02210.

Germany, G. A., G. K. Parks, M. Brittnacher, J. Cumnock, D. Lummerzheim, J. F. Spann, L. Chen, P. G. Richards, and F. J. Rich (1997), Remote determination of auroral energy characteristics during substorm activity, *Geophys. Res. Lett.*, *24*, 995–998, doi:10.1029/97GL00864.

Grocott, A., J. A. Wild, S. E. Milan, and T. K. Yeoman (2009), Superposed epoch analysis of the ionospheric convection evolution during substorms: Onset latitude dependence, *Ann. Geophys.*, *27*, 591–600, doi:10.5194/angeo-27-591-2009.

Iijima, T., and T. A. Potemra (1976), The amplitude distribution of field-aligned currents at northern high latitudes observed by Triad, *J. Geophys. Res.*, *81*, 2165–2174, doi:10.1029/JA081i013p02165.

Iijima, T., and T. A. Potemra (1978), Large-scale characteristics of field-aligned currents associated with substorms, *J. Geophys. Res.*, *83*, 599–615, doi:10.1029/JA083iA02p00599.

Kamide, Y., A. D. Richmond, and S. Matsushita (1981), Estimation of ionospheric electric fields, ionospheric currents, and field-aligned currents from ground magnetic records, *J. Geophys. Res.*, *86*, 801–813, doi:10.1029/JA086iA02p00801.

Lassen, K., and C. Danielsen (1989), Distribution of auroral arcs during quiet geomagnetic conditions, *J. Geophys. Res.*, *94*, 2587–2594, doi:10.1029/JA094iA03p02587.

Lockwood, M., and S. W. H. Cowley (1992), Ionospheric convection and the substorm cycle, *Proceedings of the International Conference on Substorms (ICS-1)*, 99–109, Kiruna, Sweden.

McPherron, R. L., C. T. Russell, and M. P. Aubry (1973), Satellite studies of magnetospheric substorms on August 15, 1968. 9. Phenomenological model for substorms, *J. Geophys. Res.*, *78*, 3131–3149, doi:10.1029/JA078i016p03131.

Milan, S. E., M. Lester, S. W. H. Cowley, K. Oksavik, M. Brittnacher, R. A. Greenwald, G. Sofko, and J. Villain (2003), Variations in the polar cap area during two substorm cycles, *Ann. Geophys.*, *21*, 1121–1140, doi:10.5194/angeo-21-1121-2003.

Milan, S. E., G. Provan, and B. Hubert (2007), Magnetic flux transport in the Dungey cycle: A survey of dayside and nightside reconnection rates, *J. Geophys. Res.*, *112*, A01209, doi:10.1029/2006JA011642.

Milan, S. E., P. D. Boakes, and B. Hubert (2008), Response of the expanding/contracting polar cap to weak and strong solar wind driving: Implications for substorm onset, *J. Geophys. Res.*, *113*, A09215, doi:10.1029/2008JA013340.

Milan, S. E., A. Grocott, C. Forsyth, S. M. Imber, P. D. Boakes, and B. Hubert (2009), A superposed epoch analysis of auroral evolution during substorm growth, onset and recovery: open magnetic flux control of substorm intensity, *Ann. Geophys.*, *27*, 659–668, doi:10.5194/angeo-27-659-2009.

Milan, S. E., J. S. Gosling, and B. Hubert (2012), Relationship between interplanetary parameters and the magnetopause reconnection rate quantified from observations of the expanding polar cap, *J. Geophys. Res.*, *117*, A03226, doi:10.1029/2011JA017082.

Mishin, V. M. (1990), The magnetogram inversion technique and some applications, *Space Sci. Rev.*, *53*, 83–163, doi:10.1007/BF00217429.

Newell, P. T., Y. I. Feldstein, Y. I. Galperin, and C.-I. Meng (1996), Morphology of nightside precipitation, *J. Geophys. Res.*, *101*, 10,737–10,748, doi:10.1029/95JA03516.

Ohtani, S., G. Ueno, T. Higuchi, and H. Kawano (2005), Annual and semiannual variations of the location and intensity of large-scale field-aligned currents, *J. Geophys. Res.*, *110*, A01216, doi:10.1029/2004JA010634.

Ohtani, S., S. Wing, P. T. Newell, and T. Higuchi (2010), Locations of night-side precipitation boundaries relative to R2 and R1 currents, *Journal of Geophysical Research*, *115*, A10233, doi:10.1029/2010JA015444.

Siscoe, G. L., and T. S. Huang (1985), Polar cap inflation and deflation, *J. Geophys. Res.*, *90*, 543–547, doi:10.1029/JA090iA01p00543.

Wing, S., P. T. Newell, and T. G. Onsager (1996), Modeling the entry of magnetosheath electrons into the dayside ionosphere, *J. Geophys. Res.*, *101*, 13,155–13,168, doi:10.1029/96JA00395.

Wing, S., P. T. Newell, and J. M. Ruohoniemi (2001), Double cusp: Model prediction and observational verification, *J. Geophys. Res.*, *106*, 25,571–25,594, doi:10.1029/2000JA000402.

Wing, S., P. T. Newell, and C.-I. Meng (2005), Cusp modeling and observations at low altitude, *Surv. Geophys.*, *26*, 341–367, doi:10.1007/s10712-005-1886-0.

Wing, S., S.-i. Ohtani, P. T. Newell, T. Higuchi, G. Ueno, and J. M. Weygand (2010), Dayside field-aligned current source regions, *J. Geophys. Res.*, *115*, A12215, doi:10.1029/2010JA015837.